ISSN 0030-770X, Volume 74, Combined 3-4

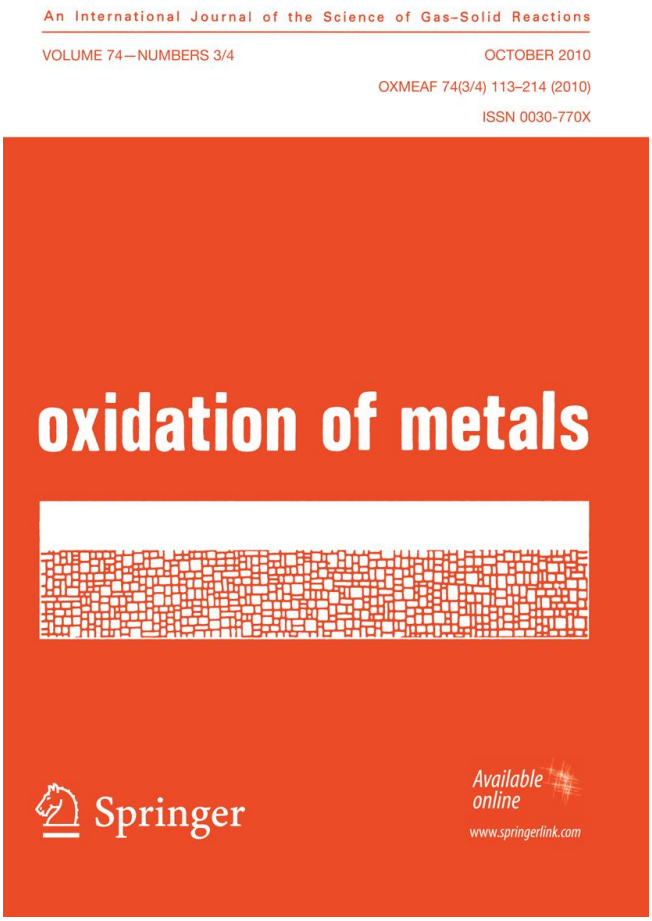

Oxid Met (2010) 74:193–203
DOI 10.1007/s11085-010-9208-4

ORIGINAL PAPER

Characterization and Oxidation Behavior of Rayon-Derived Carbon Fibers

Nathan Jacobson · David Hull

Received: 20 July 2010 / Revised: 10 August 2010 / Published online: 24 August 2010

Abstract Rayon-derived fibers are the central constituent of reinforced carbon/carbon (RCC) composites. Optical, scanning electron, and transmission electron microscopy were used to characterize the as-fabricated fibers and the fibers after oxidation. Oxidation rates were measured with weight loss techniques in air and oxygen. The as-received fibers are ~ 10 μm in diameter and characterized by grooves or crenulations around the edges. Below 800 °C, in the reaction-controlled region, preferential attack began in the crenulations and appeared to occur down fissures in the fibers.

Keywords Carbon · Carbon/carbon · Composite · Oxidation

Introduction

A rayon-derived carbon fiber/carbon composite is used as the heat shield in the Space Shuttle Orbiter [1]. These rayon-derived fibers are woven into a cloth which is formed in a two-dimensional lay-up for the carbon/carbon composite. The lay-up is then repeatedly infiltrated with a liquid carbon precursor to fill porosity, forming the reinforced carbon/carbon (RCC) composite.

High temperature carbon fibers are fabricated from rayon (cellulose), pitch, or polyacrylonitrile (PAN) precursors. Today the majority of carbon fibers are from PAN precursors. The rayon-derived fibers are a first generation fiber, however they have performed well on the Orbiter for many years. Their thermal expansion characteristics also allow application of adherent, relatively thick oxidation protection coatings.

N. Jacobson (✉) · D. Hull
NASA Glenn Research Center, Cleveland, OH 44135, USA
e-mail: nathan.s.jacobson@nasa.gov

Due to the importance of RCC to NASA's missions, several aspects of oxidation behavior of the entire composite have been studied. These include diffusion-controlled oxidation of the composite through coating pinholes [2] and coating cracks [3–5] and morphology of oxidation damage in the composite [6]. In this study, we focus only on the constituent fibers.

The oxidation of carbon in various forms has been extensively studied [7–14]. In general oxidation of carbon occurs in the following steps:

1. Diffusion of oxygen to the active sites on carbon. This diffusion may occur either through a stagnant boundary layer, through a protective coating, or both.
2. Reaction of oxygen at the active site generating CO or CO_2 and
3. Diffusion of CO or CO_2 gas away from the sample.

Generally measurable rates of oxidation begin at ~400 °C and are initially rate controlled by the chemical reaction step [7]. This reaction regime is characterized by a strong Arrhenius temperature dependence and preferential attack morphology. The reaction rates, activation energies, and attack morphology are all dependent on the type of carbon. Above 800–1000 °C, the rate-controlling step is diffusion of the gas phase reactant to the carbon or gas phase product away from the carbon. This is characterized by a weak temperature dependence and uniform attack of the carbon. This transition from reaction-control to diffusion-control is a critical feature of carbon oxidation and has been discussed by a number of investigators [7–10]. However it has not been measured under laboratory conditions for the rayon-derived fibers in RCC.

As noted, in the reaction-controlled regime, the attack morphology depends on the type of carbon. The specific structure, texture, and impurity levels all influence this morphology [7]. There are numerous studies of reaction-controlled oxidation of carbon/carbon in the literature [11–13]. Oxidation occurs preferentially along the fiber axis at the fiber/matrix interface. When fiber ends are exposed, oxidation leads to a pointed fiber morphology [13].

Ismail [10] has studied the structure and oxidation properties of carbonized rayon-derived fibers, pitch based fibers, and PAN fibers. The carbonized rayon-derived fibers had the highest porosity. The Arrhenius plots for oxidation rates for the pitch-based fibers and rayon-derived fibers showed a change in slope at 850 °C, indicating a change in mechanism from reaction control to diffusion control. This contrasts with the PAN based fibers which showed no break in slope. Reaction rates for the rayon-derived fibers also correlated to alkali content, which the author indicates catalyzes the oxidation reaction.

Lamouroux et al. [14] have done an elegant study of oxidation of T-300 carbon fibers (PAN derived fiber, made by Toray, Japan). The observed oxidation behavior is correlated with the microstructural features of the fiber. The T-300 fibers are 6–8 μm in diameter with an outer nano-porous region, an inner ring of more crystalline carbon material, and a core somewhat similar to the outer region. The outer regions are observed to consistently oxidize faster than then the inner regions.

In this study, the rayon-derived fibers are characterized. Oxidation kinetics are reported for the fiber cloths and the transition from reaction-control to diffusion-control oxidation is determined. The fibers are characterized in their as-received and

post-oxidation states. Particular attention is given to selective attack observed in the reaction control regime. An unexpected mode of attack of the rayon-derived fibers is reported.

Experimental

Fibers in the form of a cloth were oxidized in a thermogravimetric apparatus (TGA). This consisted of a vertical tube furnace with a 5 cm hot zone and microbalance (Cahn 1000). Cloth samples of ~0.30 g were placed in an alumina cup with slots cut in the bottom for gas flow. Tests were done in oxygen or air at a flow rate of 100 cc/min. Weight change and temperature data was collected with an automated collection system. Rates were taken as the instantaneous slope at 50% consumption, according to convention [14] for carbon materials. Oxidation rates were measured every 100° between 500 and 1200 °C.

Fibers were mounted in epoxy and polished with diamond pastes for examination of both the as-fabricated and post-oxidation samples. Optical micrographs were taken with a Reichert MeF3A (Optronics) system with a digital camera. Scanning electron microscopy was done with a Hitachi S4700 Cold Field Emission Scanning Electron Microscope (FE-SEM). A thin carbon film was evaporated onto the surface of mounted and polished samples to provide conductivity for the FE-SEM examination.

The rayon-derived fibers were examined with a Philips CM200 transmission electron microscope (TEM) operating at 200 kV. The objective was to characterize the structure from the outer edge of the fiber to the inner core in relation to porosity, crystallinity, and general organization of the graphite layers.

TEM sample preparation proved to be a major challenge. It was not possible to prepare individual fibers as any type of clamping material such as epoxy or silicon milled faster than the fibers. So the composite with carbon fibers in a carbon matrix was used. The carbon matrix milled at about the same rate as the fibers and thus held the fiber in place. Standard sample preparation methods were then used. A ~1 mm thick slice was taken from the composite and polished from both cut surfaces to 150 μm thickness with diamond mylar films with decreasing grit sizes of 6, 3, and 1 μm. The thickness was further reduced by dimple grinding using a Gatan 656 Dimple Grinder to 20 μm thickness in the center and then ion milled with Ar ions at 5 kV and 8° impingment angle (Gatan PIPS). One specimen was prepared with a Hitachi FB-2100 focused ion beam system (FIB).

Results and Discussion

Characterization of the As-Received Fibers

Figure 1 is a FE-SEM longitudinal view of a rayon-derived fiber. The rounded particulates on the surface are all carbon. Note the grooves or crenulations in the fibers, which are more apparent in the FIB cross section as imaged in the TEM

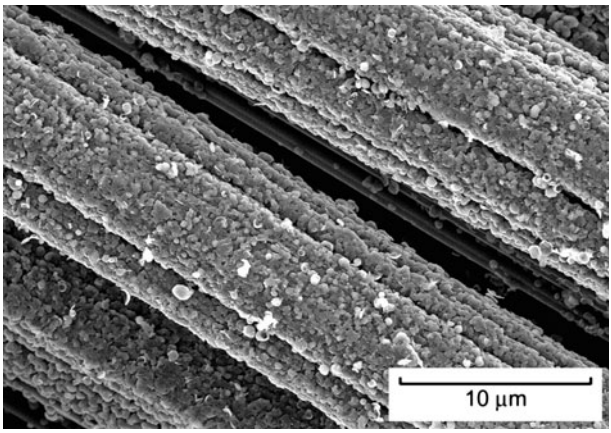

Fig. 1 FE-SEM micrograph of rayon-derived fibers

(Fig. 2a). This is characteristic of wet-spun fibers [15]. Selected area diffraction (SAD) of the fiber shows the classical ring pattern consistent with randomly oriented fine crystallites (Fig. 2b). The uniformity of the fiber is apparent in both bright and dark field TEM imaging (Fig. 2c and d, respectively). Dark field TEM imaging further shows the randomly ordered fine graphite crystallites in more detail (Fig. 2d) from the fiber edge to the fiber center.

Bright field imaging across the diameter of the fiber showed no dramatic differences in the arrangement of the carbon layers, except for small ($\sim$50 nm) graphite rings surrounding pores (Fig. 3a). The center of the ring is lighter indicating less material in the beam path, which is indicative of a pore. The pores appear to be randomly scattered throughout the fiber. High-resolution lattice imaging shows the 5–10 layers of carbon forming the ring around these pores (Fig. 3b).

Figure 4 is an electron micrograph showing the longitudinal fibers actually in a carbon matrix. Note again the crenulations and the variation in fiber diameters. In summary, rayon-derived fibers appear to have a surface dominated by crenulations and randomly oriented fine crystallites throughout. There are also randomly distributed nano-pores throughout the fiber. This contrasts with PAN derived fibers, which show a much different behavior with a porous outer shell, an inner crystallized ring concentric to the outer diameter, and a nano-porous inner core [14].

Oxidation Rates and Post-Oxidation Morphology

A typical oxidation weight loss curve for the fiber cloth is shown in Fig. 5. Weight loss was linear and a rate was easily determined at 50% weight loss. The time to achieve 50% weight loss varied from 7.5 days at 500 °C to about 1 h at 1200 °C. An Arrhenius plot for the fiber cloth is shown in Fig. 6. This is the type of Arrhenius behavior is expected for carbon and carbon fibers [7–10, 14]. The kinetics at low temperatures ($T < 800$ °C) show a strong temperature dependence, whereas the kinetics at high temperatures ($T > 800$ °C) show a weak temperature dependence.

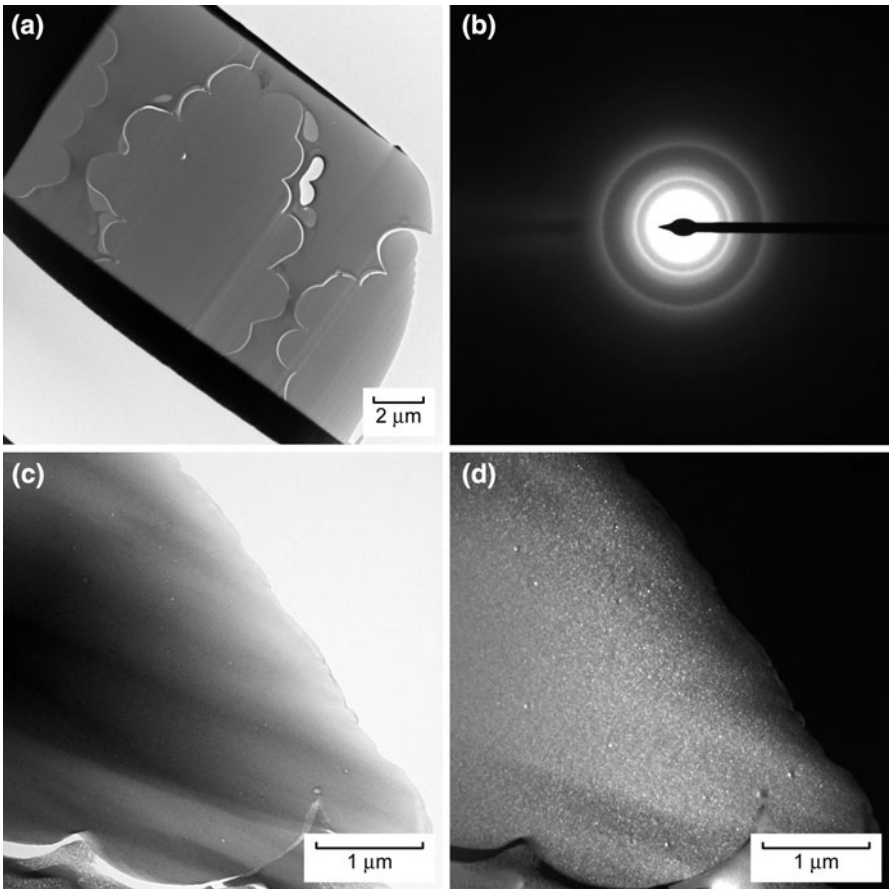

Fig. 2 TEM of as received rayon-derived fiber prepared by **a** FIB **b** selected area electron diffraction (SAD) pattern showing random crystallinity by continuous ring pattern. **c** Bright field image of conventional ion milled as received rayon-derived fiber. **d** Dark field image showing uniform random crystallinity

In the low temperature region, the rate-controlling process is a chemical reaction, which necessarily shows an exponential dependence on temperature. In the high temperature region, the rate controlling process is diffusion of the reactants to the sample or diffusion of the products away from the sample. Here the temperature dependence is determined by the gas phase diffusion coefficient, which is dependent on temperature with an exponent of 1.5 [16].

Figure 6 shows oxidation rates in both air and oxygen. Note the rates in air are slower due to the dependence of rate on oxygen partial pressure. While there are not enough data to obtain a quantitative partial pressure dependence, this approximately proportional decrease in rates with pressure is expected for the diffusion-control regime [7]. The partial pressure dependence for the reaction control regime depends on the particular reaction mechanism [7], but is expected to decrease with decreasing partial pressure of oxygen.

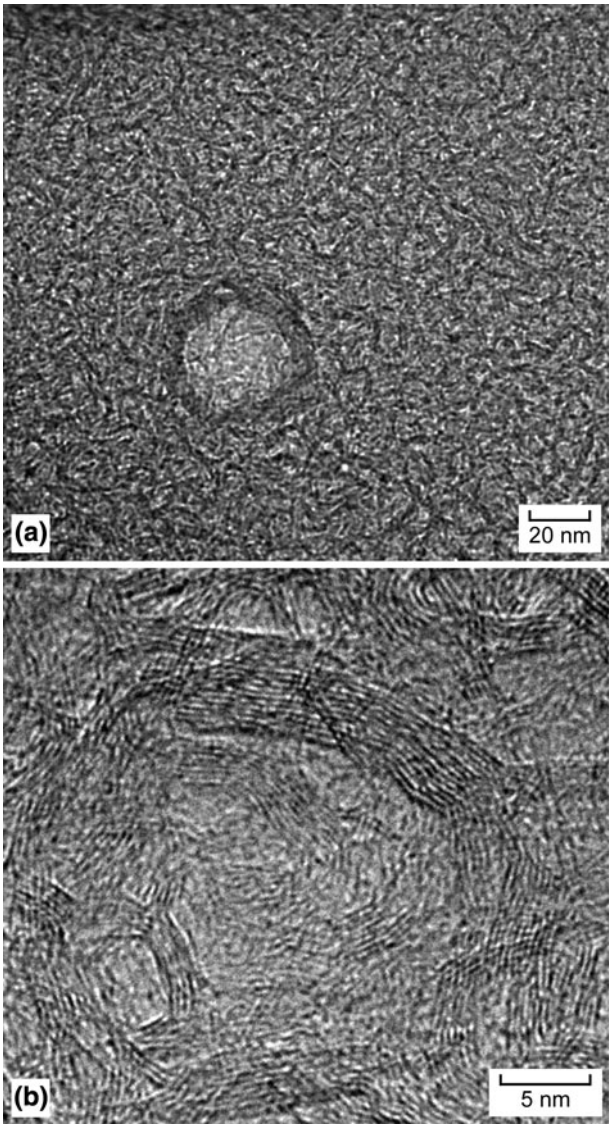

Fig. 3 TEM bright field image showing **a** ~50 nm graphite ring surrounding a pore and **b** high-resolution lattice imaging showing graphite ring structure

Also shown in Fig. 6 are the data for T-300 fiber [17]. Note in the diffusion-control regime, the data are nearly identical to the rayon-derived fiber, as expected. The T-300 fibers do not show the two regimes, but rather remains in the diffusion-control regime for the entire temperature range. This has been observed by other investigators and is explained by a rapid increase in porosity at the beginning of oxidation, creating a structure where gas phase diffusion is always limited by these pores [10].

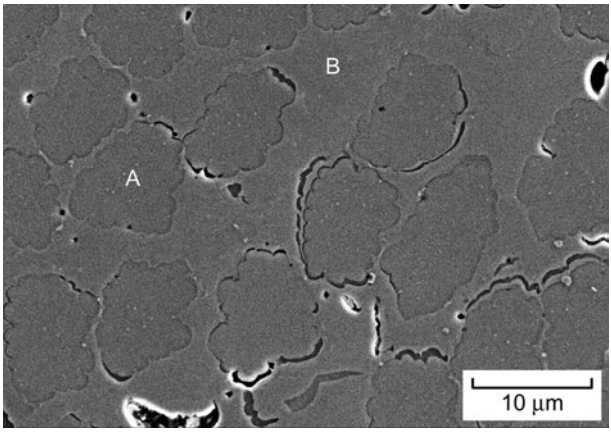

Fig. 4 Rayon-derived fibers (A) in a carbon matrix (B)

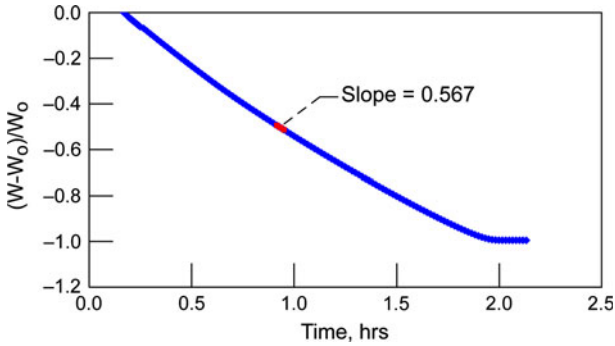

Fig. 5 Typical weight loss curve for rayon-derived carbon fiber cloth at 900 °C in air. Note the specimen is consumed at ~2 h

As discussed, oxidation of carbon fibers occurs preferentially along the edges [6, 13] and leads to a general thinning of the fibers. This occurs in both the reaction-controlled and diffusion-controlled regimes. Figure 7 is a fiber cloth oxidized at 700 °C for 1.1 h. The fibers show a clear reduction in diameter from ~10 µm from the as-received fibers to ~5 µm for the oxidized fibers. The small rounded grains are the surface are gone, leaving a smoother surface with the grooves clearly delineated. Note also there are small cavities on the randomly spaced on the edges of some fibers. The diameter reduction as well as the cavities will have significant impact on the strength of these fibers.

An examination of the sample after 50% weight loss (6.5 h at 600 °C/air) showed selective attack in the 'valley' of the crenulations and into the fissures of the fiber. This is shown in the polished cross section in Fig. 8. Fracture sections were also examined, as shown in Fig. 9a–c. Figure 9a clearly shows the layer with the sub-micron rounded grains is removed, revealing the smooth, grooved surface as shown

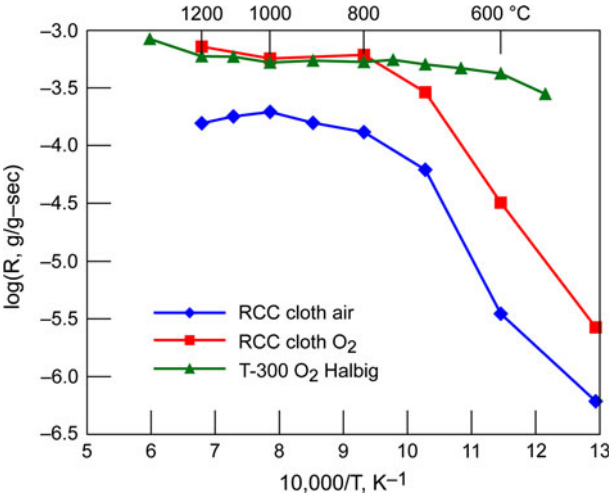

Fig. 6 Arrhenius plot for oxidation of RCC cloth compared to T-300 carbon fibers

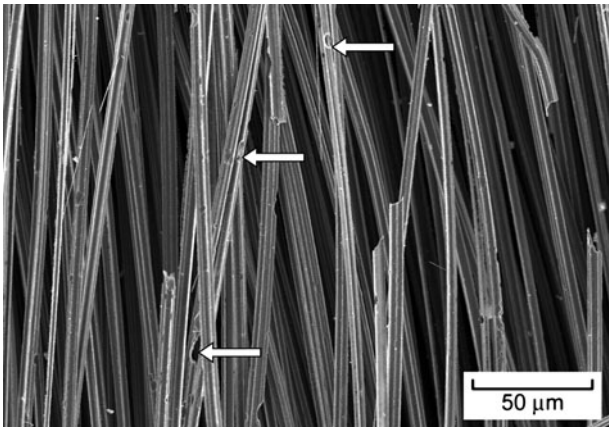

Fig. 7 Rayon-derived fibers oxidized at 700 °C for 1.1 h

in Fig. 9b. Figure 9b and c clearly show attack at the base of the grooves into the fibers, as observed in the cross sections.

This type of attack was unexpected and previous studies have indicated uniform attack along fiber edges [6, 13]. The micrographs suggest that the attack begins in the 'valley' of one of the crenulations and proceeds to open a fissure progressing through the full diameter of the fiber. Higher magnification TEM micrographs show multiple fissures with various orientations, as shown in Fig. 10a. Figure 10b shows material exuding from the fissure. It may be that some type of high volatility carbon-containing material is released from these fibers on heat-up in oxidizing environments, which leads to the fissures. These fine details were not observed in the as-fabricated specimens (Fig. 2a–d).

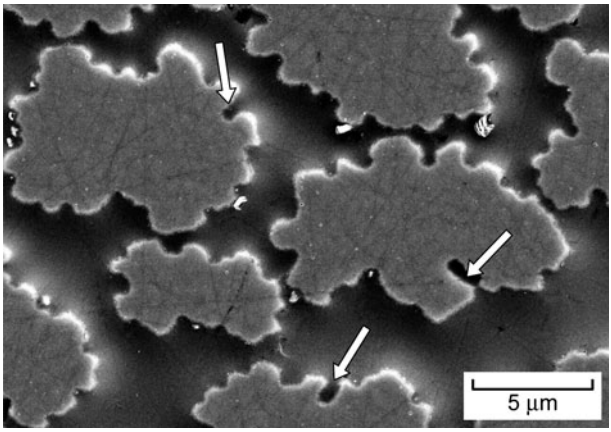

Fig. 8 FE-SEM of rayon-derived fibers oxidized at 600 °C for 6.5 h in air. Note the fibers are showing initial signs of attack in the grooves

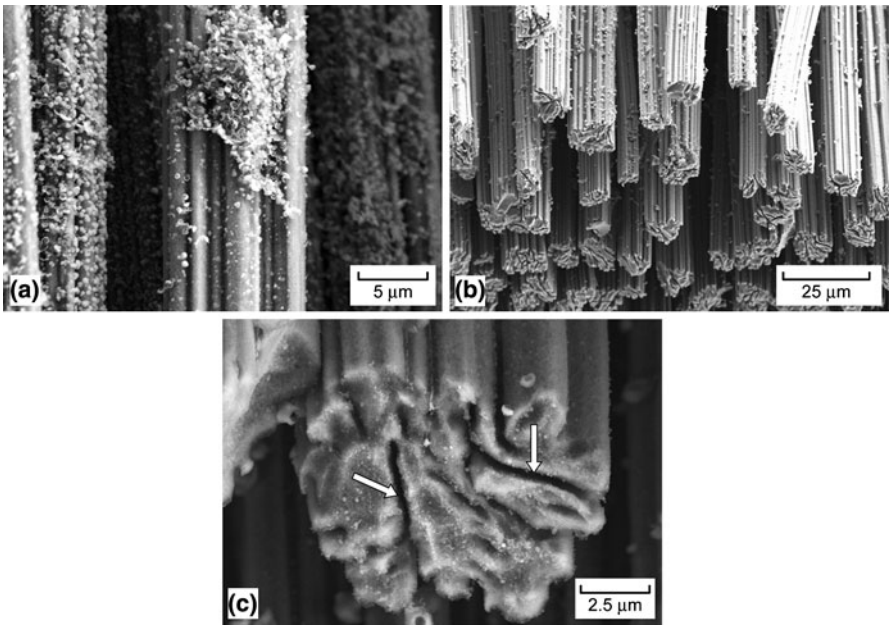

Fig. 9 FE-SEM of fracture section of sample oxidized at 600 °C for 6.5 h. **a** Fibers showing partial removal of the outer layer of rounded grains. **b** Fiber bundle showing numerous fissures. **c** Close up of fissures

Summary and Conclusions

The oxidation of the rayon-derived carbon fibers has been discussed, with particular emphasis on the reaction control regime and transition to diffusion-control. The as-fabricated rayon-derived fibers showed ~ 1 μm crenulations and hollow

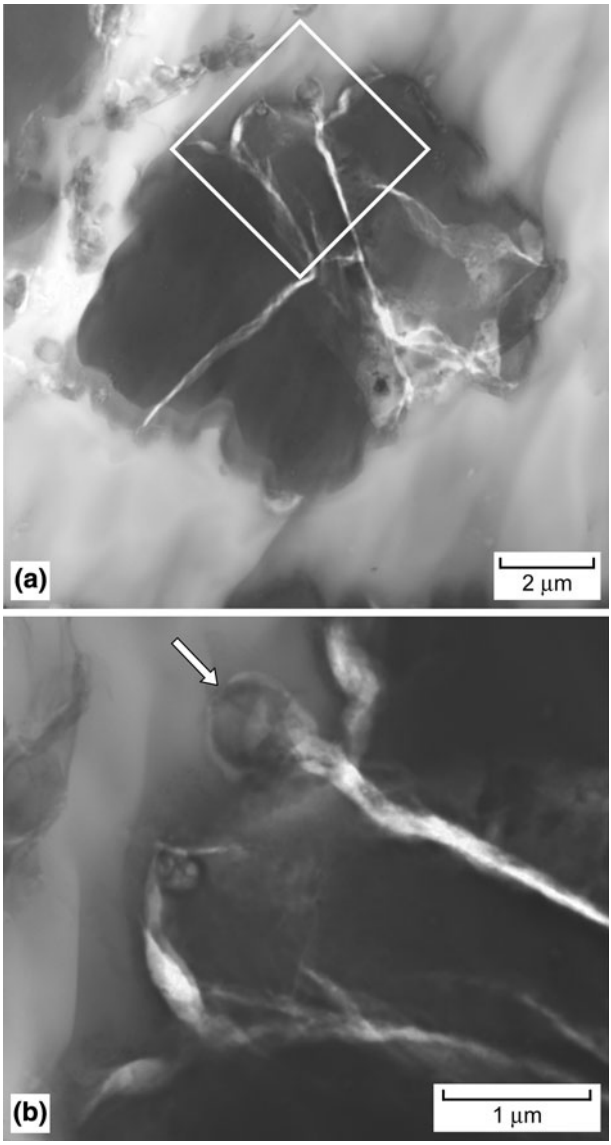

Fig. 10 Sample oxidized at 600 °C for 6.5 h. **a** TEM view shows numerous fissures. **b** Higher magnification shows fine details of oxidation fissures and material exuding from fissure

nano-spheres lined with planes of graphite. Otherwise the fibers appeared to have a uniform microstructure throughout.

Oxidation was studied from 500 to 1200 °C in oxygen and air. Reaction-controlled oxidation continues to about 800 °C. In this regime, the matrix oxidized preferentially to the fibers and the fibers showed attack down fissures, deep into the individual fibers.

Acknowledgment It is a pleasure to thank Donald Humphrey and Terry McCue, both of ASRC/NASA Glenn Research Center for the kinetic measurements and electron microscopy respectively. Helpful discussions with Dr. E. Opila of NASA Glenn are appreciated.

References

1. D. M. Curry, J. W. Latchem, and G. B. Wisenhunt, *21st AIAA Aerospace Sciences Meeting* (AIAA, 1983).
2. N. S. Jacobson, T. A. Leonhardt, D. M. Curry, and R. A. Rapp, *Carbon* **37**, 411 (1999).
3. J. E. Medford, *Prediction of Oxidation Performance of Reinforced Carbond-Carbon Material for Space Shuttle Leading Edges*. Paper 75-730 (AIAA 10th Thermophysics Conference, Denver, CO, May 27–29, 1975).
4. J. E. Medford, *Prediction of In-Depth Oxidation Distribution of Reinforced Carbon-Carbon Material for Space Shuttle Leading Edges*. Paper 77-783 (AIAA 12th Thermophysics Conferencerence, June 27–29, 1977).
5. N. S. Jacobson, D. J. Roth, R. W. Rauser, J. D. Cawley, and D. M. Curry, *Surface and Coatings Technology* **203**, 372 (2008).
6. N. S. Jacobson and D. M. Curry, *Carbon* **44**, 1142 (2006).
7. P. L. Walker, Jr., F. Rusinko, Jr., and L. G. Austin, in *Advances in Catalysis and Related Subjects*, eds. P. D. Eley, P. W. Selwood, and P. B. Weisz, Vol. XI (Academic Press, New York, 1959), p. 133.
8. K. S. Goto, K. H. Han, and G. R. St. Pierre, *Transactions ISIJ* **26**, 597 (1986).
9. D. W. McKee, *Carbon* **25**, 551 (1987).
10. I. M. K. Ismail, *Carbon* **29**, 777 (1991).
11. P. Crocker and B. McEnaney, *Carbon* **29**, 881 (1991).
12. J. Rodriguez-Mirasol, P. A. Thrower, and L. R. Radovic, *Carbon* **33**, 545 (1995).
13. W. H. Glime and J. D. Cawley, *Carbon* **33**, 1053 (1995).
14. F. Lamouroux, X. Bourrat, R. Naslain, and J. Sevely, *Carbon* **31**, 1273 (1993).
15. D. D. Edie and R. J. Diefendorf, Carbon Fiber Manufacturing. in *Carbon-Carbon Materials and Composites*, eds. J. D. Buckley and D. D. Edie (Noyes, Park Ridge, NJ, 1993), p. 19.
16. G. H. Geiger and D. R. Poirier, *Transport Phenomena in Metallurgy* (Addison-Wesley Publishing Co., Reading, MA, 1973).
17. M. C. Halbig and J. D. Cawley, *Modeling the Oxidation Kinetics of Continuous Carbon Fibers in a Ceramic Matrix.* NASA/TM—2000-209651 (January 2000).